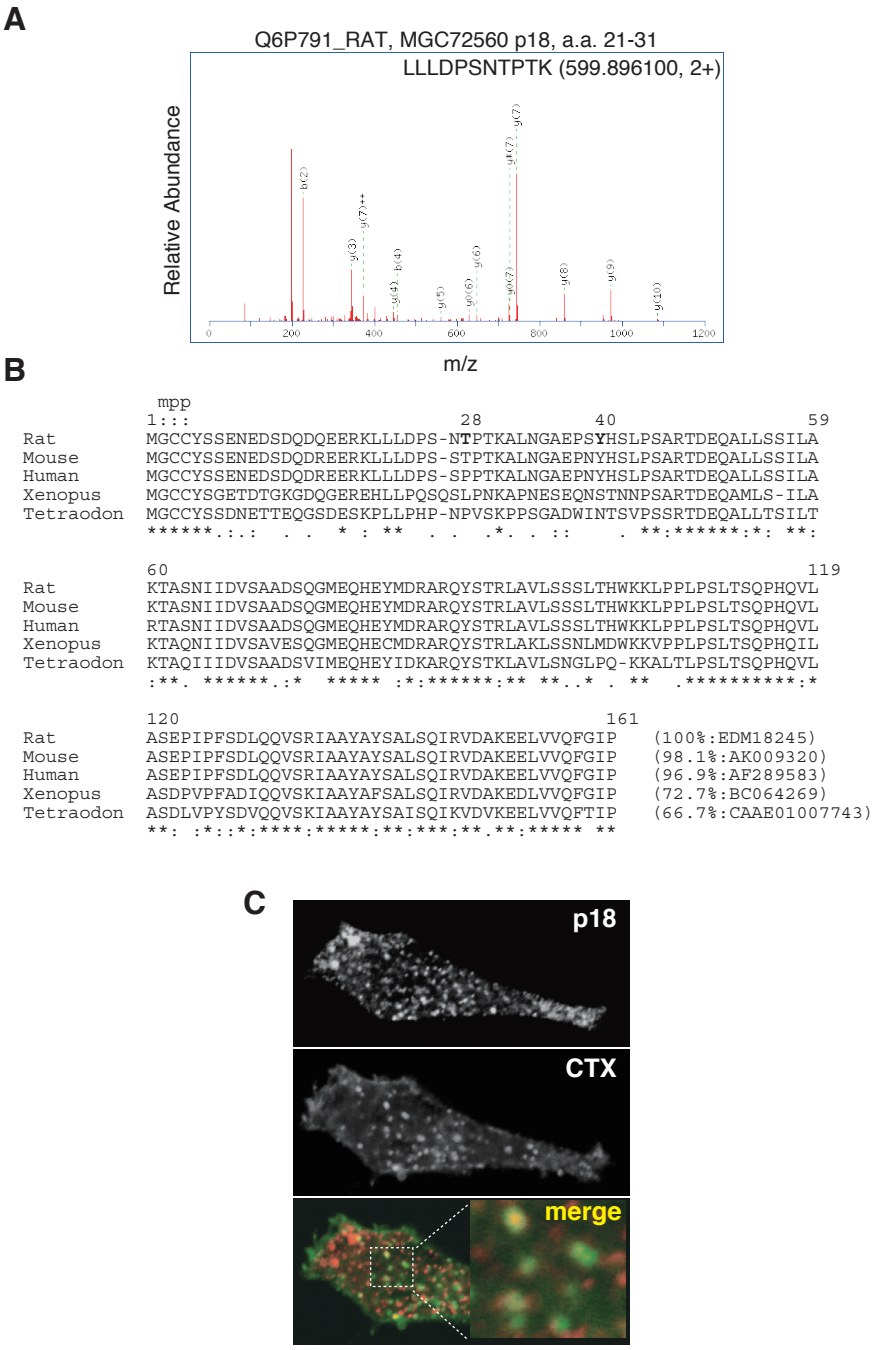

Figure S1. Identification of p18

(**A**) A representative MS/MS spectrum assigned to MGC72560. Peptide mass and valence are given in the parentheses following the peptide sequences. a.a.; amino acid number from the N- to C-terminus of the fragment. (**B**) Amino acid alignment of p18 from several vertebrates analyzed by Clustal W. Amino acid identity to rat p18 and accession numbers are shown in parentheses. (**C**) PC12 cells were stained with anti-p18 and CTX, and observed using a confocal laser-scanning microscope. An enlarged view of the white box is shown in the merged image.

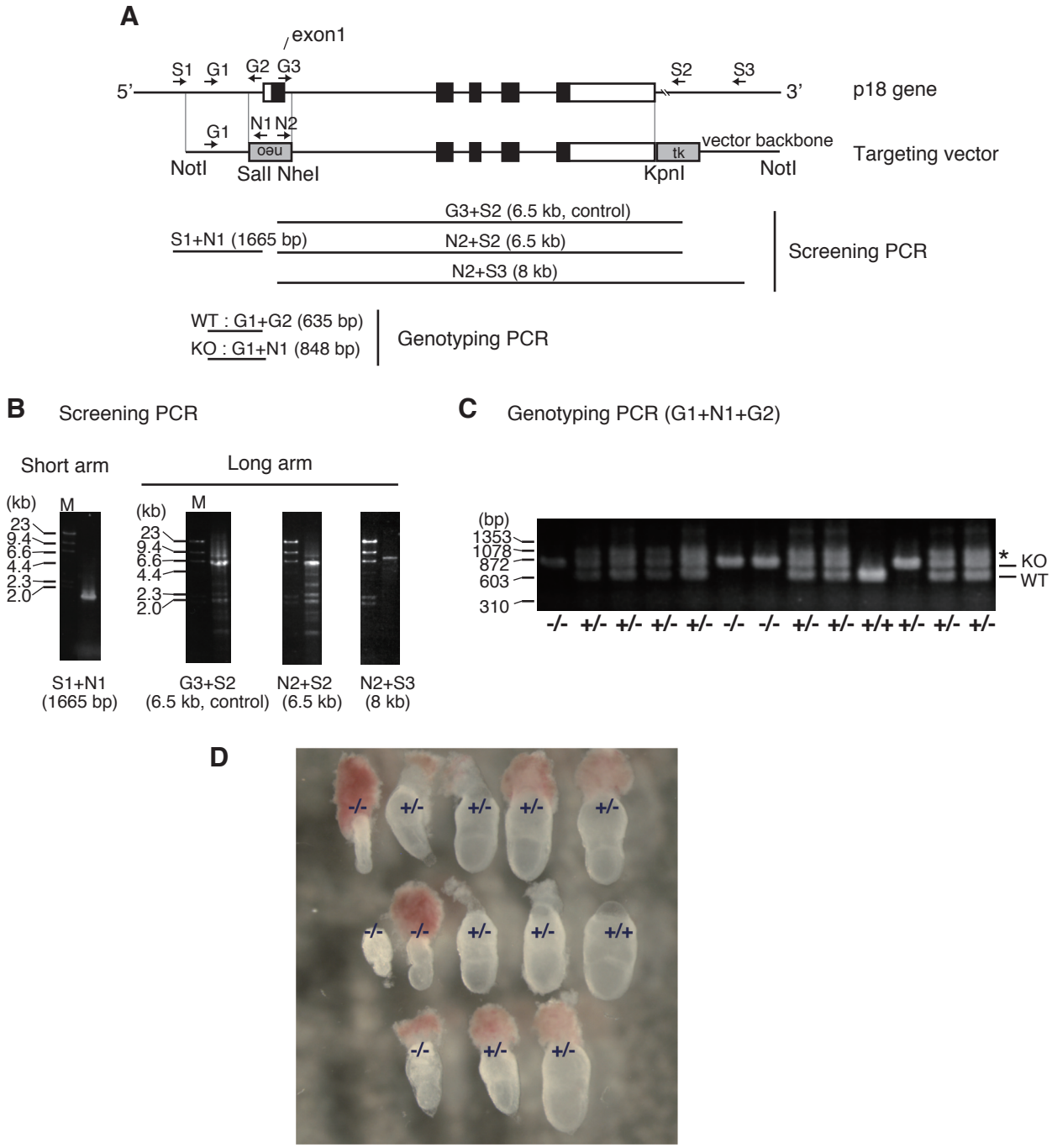

Figure S2. Generation of p18 knockout mice

(**A**) Schematic diagram of the p18 gene and targeting vector containing the locations of PCR primer sequences designed for screening (S1-N1, G3-S2, N2-S2 and N2-S3) and genotyping (G1-G2 and G1-N1). The predicted sizes of PCR products are also shown. Primer sequences are: S1 (5' -TCT GCC CAG CTA CCT ATC CAA ACT GAA CAC), G1 (5' -AAG AGA AGT GTC TGC CAT CTG CCT ACT CAG), G2 (5' -GAC AAT CGC CAA CCA ATG GAA AAG TGC GTC), N1 (5' -GCC TTC TAT CGC CTT CTT GAC GAG TTC TTC), N2 (5' -TAC CCG GTA GAA TTG ACC TGC AG), G3 (5' -AAG GCT AGC CTA GTC TTA CTT CTG CCT AGG GT), S2 (5' -GAA GTA AAG AGT GGG CAG GAC AGA) and S3 (5' -CCT CCA TGG GAA CCC CAT AG). (**B**) A representative result of PCR screening of homologous recombinant. DNA marker sizes are shown on the left side of the panels. (**C**) PCR genotyping of a litter of E7 embryos obtained from an intercross of $p18^{+/-}$ mice. An asterisk shows non-specific band given by heterozygous embryos (+/-). Loss of p18 protein in $p18^{-/-}$ embryo was confirmed by immunofluorescence analysis of tissues (Fig.2 B). RT-PCR and immunoblot analyses of $p18^{-/-}$ cells also showed that the expression of p18 transcript and protein was completely ablated by gene targeting (Fig.S3). (**D**) Gross appearances of genotyped embryos from (C). Genotype is indicated on each embryo.

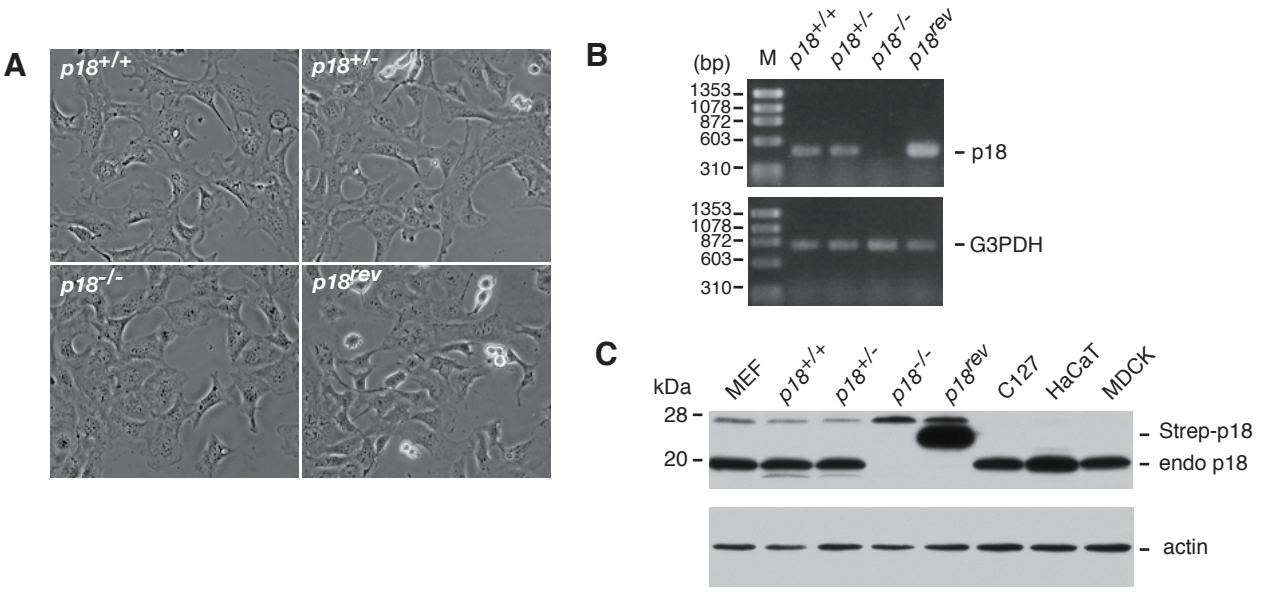

Figure S3. Establishment *p18*$^{-/-}$ and *p18*^{rev} cells

(**A**) Phase contrast images of *p18*$^{+/+}$, *p18*$^{+/-}$, *p18*$^{-/-}$ and *p18*^{rev} cells. (**B**) RT-PCR analysis of p18 expression. p18 transcripts were not detected in *p18*$^{-/-}$ cells. Transcripts of glyceraldehyde-3-phosphate dehydrogenase (G3PDH) were detected as an internal control. Primer sequences are: p18 forward (5' -ATG GGG TGC TGC TAT AGC AGC GAA), p18 reverse (5' -TCA TGG GAT CCC AAA CTG TAC AAC C), G3PDH forward (5' -ACT CCA CTC ACG GCA AAT TC) and G3PDH reverse (5' -CCC TGT TGC TGT AGC CGT AT). (**C**) Immunoblot analysis of p18 protein in the indicated cell lines. Locations of strep-tagged p18 (Strep-p18) and endogenous p18 (endo p18) are indicated. Expression of p18 protein was null in *p18*$^{-/-}$ cells. Actin was detected as loading control.

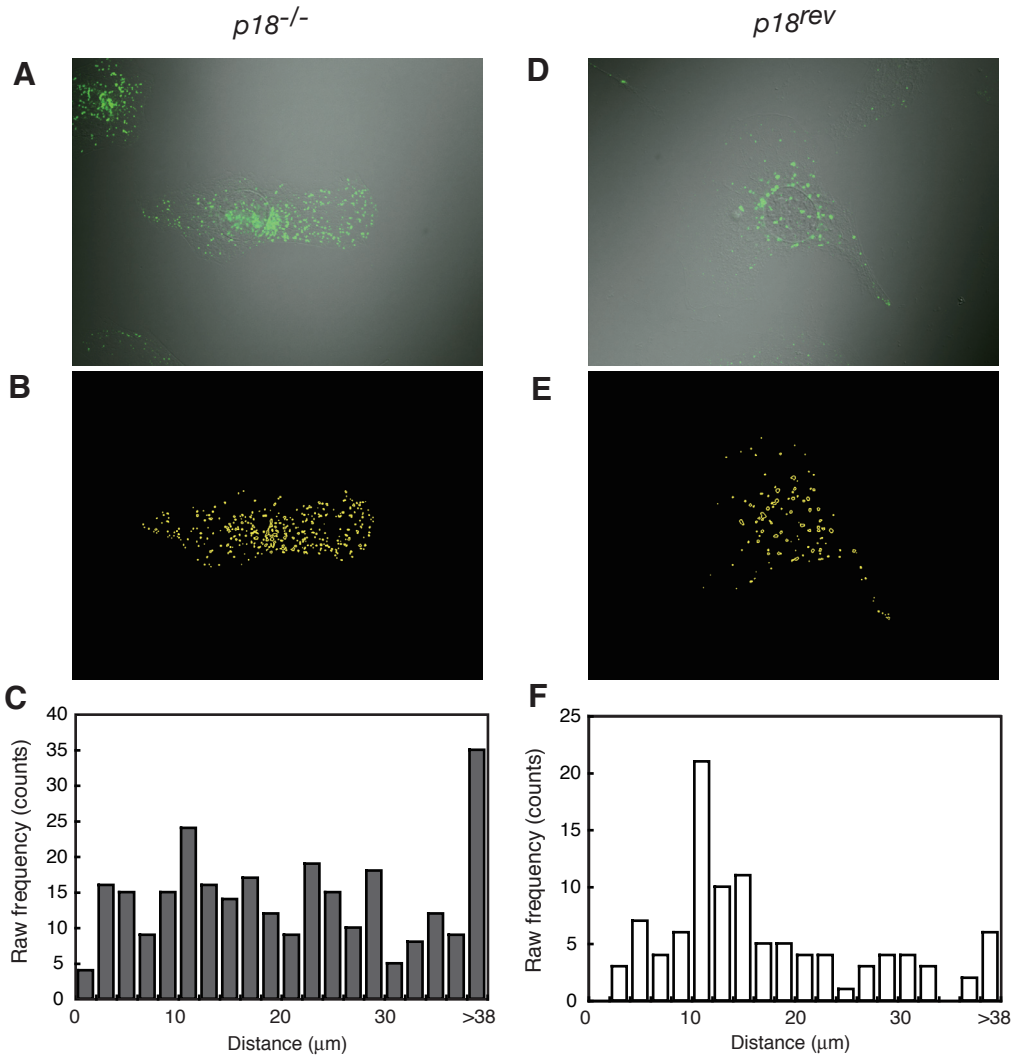

Figure S4. Analysis of LAMP-1 positive lysosome distribution

Analysis of LAMP-1 positive lysosome distribution with respect to the distance from the nucleus was performed essentially as described previously (Bohn et al, 2007). *p18*$^{-/-}$ (**A**-**C**) and *p18*^{rev} (**D**-**F**) cells were stained with anti-LAMP-1, and DIC and fluorescence images were obtained by FV1000 laser-scanning microscope with 100x objective lens (Olympus) at 16-bit data depth (**A** and **D**). Images were processed with Metamorph software (Molecular Devices). The region of nucleus was traced manually from DIC images. For LAMP-1 images, 2D deconvolution was first applied, and LAMP-1 signals were identified by thresholding the signal intensity (**B** and **E**). The location of LAMP-1 positive vesicles was recorded by region measurement function, and the center position of each vesicle was defined as center (X,Y) = location (X,Y) + width (X,Y)/2. Distance from nucleus center was calculated by Pythagoras' theorem, and the results were binned in units of 2 μm in range of 0 to 40 μm (**C** and **F**). Totally, 17 *p18*$^{-/-}$ cells and 17 *p18*^{rev} cells were processed. A X^2 independence test was done on the original data (sum of all LAMP-1-positive vesicles per bin) for *p18*$^{-/-}$ vs *p18*^{rev} cells, resulting in $p < 0.001$.

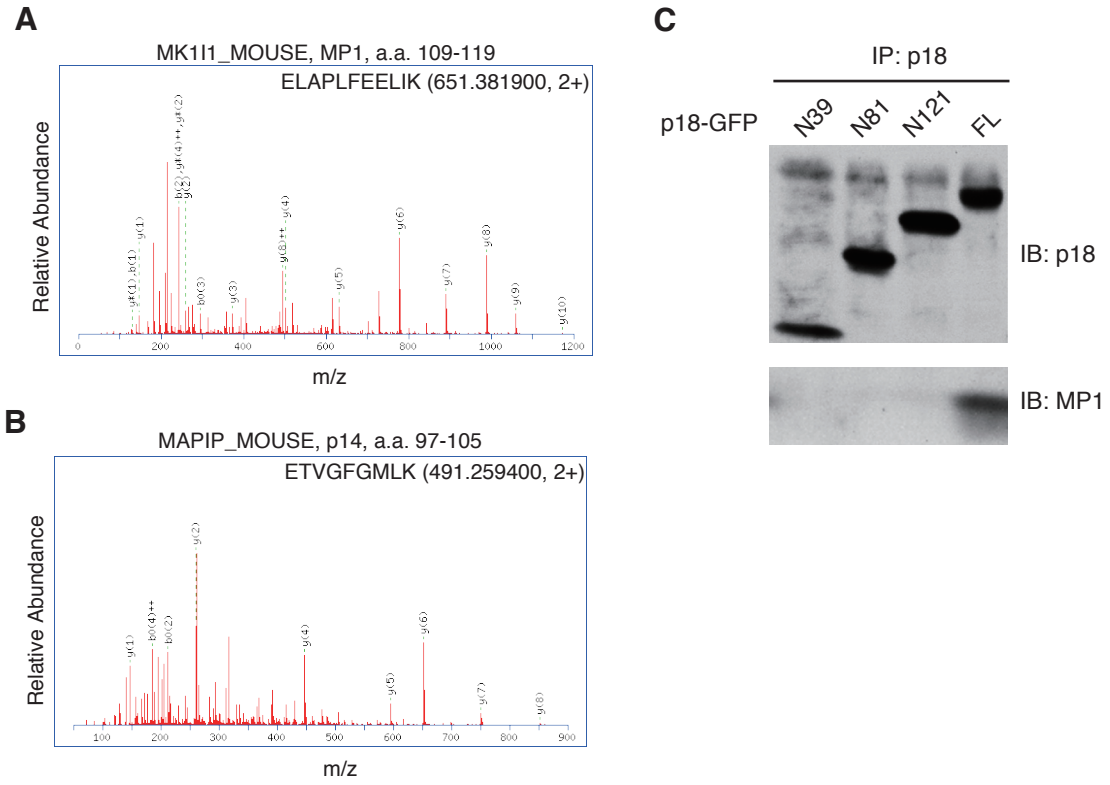

Figure S5. Identification of p14 and MP1 as binding partners of p18
(**A** and **B**) Representative MS/MS spectra assigned to MP1 (A) and p14 (B). (**C**) GFP fusion proteins containing a series of p18 deletion mutant (a.a. 1-39; p18N39, 1-81; p18N81, 1-121; p18N121, 6-161) and full length p18 (FL) were expressed in *p18*$^{-/-}$ cells, and immunoprecipitated with anti-GFP antibody, followed by immunoblotting with anti-p18 (upper panel) and anti-MP1 (lower panel) antibodies.

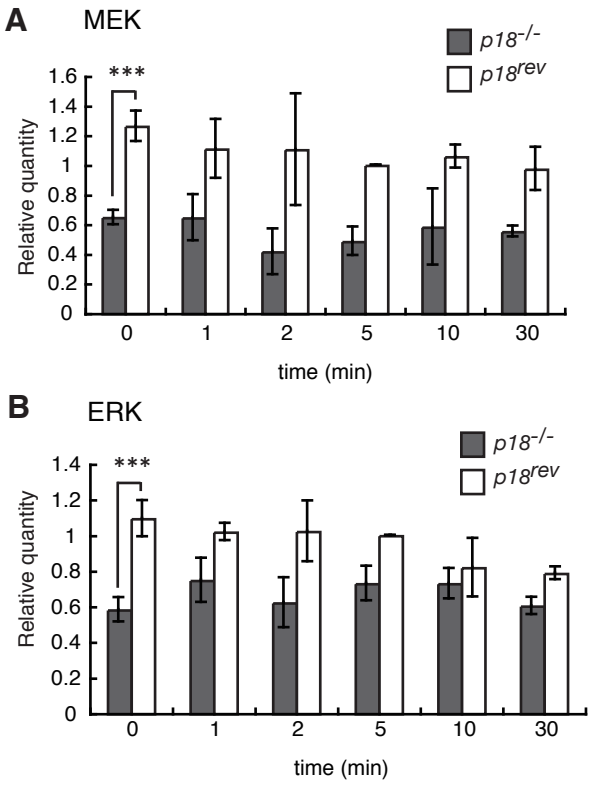

Figure S6. p18-dependent distribution of MEK and ERK to DRMs

p18^{rev} and *p18*$^{-/-}$ cells were stimulated with EGF, and the relative quantities of MEK (**A**) and ERK (**B**) in DRMs at the indicated time points were determined by immunoblotting. (**A**) Mean ± S.D. of the relative quantities of MEK in DRM fractions of *p18*^{rev} (n=4, white) and *p18*$^{-/-}$ (n=4, gray) cells are shown. Differences between groups were analyzed by using repeated measures analysis of variance (ANOVA); P=0.0068. Difference at the initial time point was analyzed by Student's t-test; ***P< 0.001. (**B**) Mean ± S.D. of the relative quantities of ERK in DRMs of *p18*^{rev} (n=4, white) and *p18*$^{-/-}$ (n=4, gray) cells are shown. Differences between groups were analyzed by using repeated measures analysis of variance (ANOVA); P=0.0026. Difference at the initial time point was analyzed by Student's t-test; ***P< 0.001.

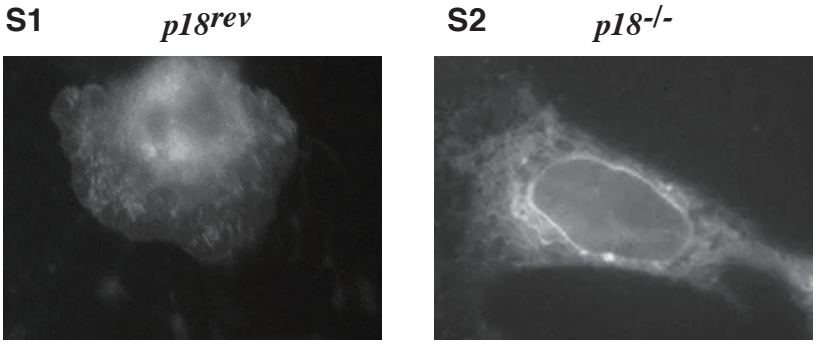

Supplemental Movie Legends

Movie S1 and S2. Time-lapse images of integrin β1 in *p18*^{rev} and *p18*$^{-/-}$ cells

QuickTime movies of *p18*^{rev} (**S1**) and *p18*$^{-/-}$ (**S2**) cells expressing integrin β1-GFP. In *p18*$^{-/-}$ cells, integrin β1 constitutively accumulates in endosomes and the endoplasmic reticulum, while *p18*^{rev} cells actively transport integrin β1 to the cell periphery and focal adhesions.